Studying the Behavior of the West End Tower with Magnetic Injections

Adrian Avila-Alvarez
Advisors: Dr. Irene Fiori, Dr. Paolo Ruggi
11, August 2014

1. General Introduction

The Virgo observatory is the largest gravitational-wave (GW) laser interferometer in Europe, with each of two arms extending to 3 km in length. As part of a collaboration with LIGO, Virgo wants to achieve its first gravitational-wave detection. Gravitational waves (GWs) are ripples in the fabric of space-time caused by extreme astrophysical processes as predicted in Albert Einstein's Theory of General Relativity. Moreover, the Virgo collaboration is installing a new interferometer, named Advanced Virgo (AdV), which will comprise most of the present infrastructure of Virgo, with the exception of 3 basic upgrades. These upgrades include: a laser that is 10 times as powerful as the predecessor, new mirrors with improved surface quality to increase arms' finesse, and enhanced-quality, monolithic mirror-suspension system with quarts fibers to drastically reduce thermal noise. These upgrades will increase Virgo's sensitivity to GW signals by roughly 10 times and thus allow to explore a volume of the universe 1000 times greater, or in other words increase detection rate probability by a factor of 10. GW signals from a frequency range of 10 Hz to 10 kHz are detected by measuring the differential length change of the two arms; therefore, any mirror displacement not due to GWs is denoted as "noise". In addition, the seismic noise due to the ground/Earth is reduced or shielded by suspending the mirrors in a 10-meter high multistage, active-controlled pendulum called the Super Attenuator (SA) system. Each SA is encapsulated by cylinder-shaped vacuum tanks, called "towers", whose structure will be described in more detail later into the document.

On the other hand, AdV's sensitivity might be influenced by (hopefully not limited to) the effects of environmental noise – particularly electromagnetic (EM) noise. Four tiny magnets (SmCo, 1.5mm^3 volume, 1T residual magnetic induction) attached in cross configuration onto the mirror back surface (and work as actuators) fall victims to the presence of EM noise. These magnetic actuators can couple to local magnetic fields and/or gradients and displace the mirrors, thus mimicking GW signals. The sources of ambient magnetic noise are distributed throughout the experimental hall and include: electronics boards, pumps, lights, electrical power circuits, and in principle any wire where current flows. At the towers' location, care has been taken not to place the sources listed (except for vacuum pumps) in close proximity; we assume that they are sufficiently far away (compared to their source size) to the point where their magnetic field lines are roughly parallel (no gradient). Unfortunately, Eddy currents induced by the conductive nature of materials in proximity to the magnetic actuators are not as easily measured as those sources in the hall. Because of Eddy currents, external magnetic fields (those that reside in the hall) are spatially distorted and changed in magnitude by the presence of conductive parts. The two most conductive materials are the "cages" and the towers. The

"cage" is a 50-kg steel and aluminum frame that surrounds each mirror test mass and is as close as about 10 cm away from the mirror, while the 13-ton tower walls composed of steel are about 1 meter away from the mirror. Since the mirror location is not accessible during AdV operation, measurements and information are going to be collected while AdV mirrors are not yet installed and towers are in-air. Data collected will allow us to predict the magnetic field and gradients at mirror magnets' position starting from measurements of the field in the hall. While the "cage" distortion effect is being studied by the EM Comsol simulation [ref1], the tower has a more complex design and thus the most reliable approach is to conduct experimental measurements. This is the subject of my work.

2. Technical Introduction

2.1. Strain Noise due to Magnetic Fields and Gradients

There are two kinds of forces produced by the coupling of external magnetic fields and the magnetic actuators:

- Torques associated to magnetic fields : $\vec{\tau} = \sum_i \overrightarrow{\mu_i} \times \overrightarrow{B_i}$
- Forces associated to magnetic gradients: $\vec{F} = \sum_i \vec{\nabla}(\overrightarrow{\mu_i} \cdot \overrightarrow{B_i})$

where "*i*" represents each mirror magnet (*i* = 1,…,4). Note that only mirror displacements along z (laser beam direction of West or North arm) are of concern since they cause differential length changes which mimic GW strain. Furthermore, the displacement associated with forces due to magnetic gradients is:

$$z_{mirror} = \frac{F_z}{M \cdot (2\pi f)^2}$$

where M is the mass of the mirror (40 kg) and the strain noise mimicking a GW signal is :

$$h = \frac{z_{mirror}}{L_0}$$

where L_0 is the unperturbed arm length of 3 km. In order to make out the strain noise and make a projection to see where it stands with respect to AdV design sensitivity, we must understand the magnetic fields (case of torques) and gradients (case of forces) at the mirror magnets' position; hence, examining the "behavior" of the towers subject to external fields. In this document, we will investigate the behavior of the West End (WE) tower.

2.2. West End Tower

The WE tower is a 10-meter tall, 13-ton vacuum chamber that encloses the SA-mirror system. It's cylindrical in shape and is composed of a special steel called 340L. Its diameter stretches to 2 meters and is 1.5 cm thick. Additionally, the lower-half of the WE tower is surrounded by a box-like perimeter referred to as the "oven", which is made of two layers of steel (type Fe360 enriched in iron content) 1.5 mm thick plus a glass fiber sheet. The "oven"

was used in the past by Virgo Plus (older design of Virgo) as thermal isolation for the lower part of the tower; although, for technical reasons (lack of space for the installation of new optical benches for AdV), each oven will be removed. We wish to also understand their role with EM noise.

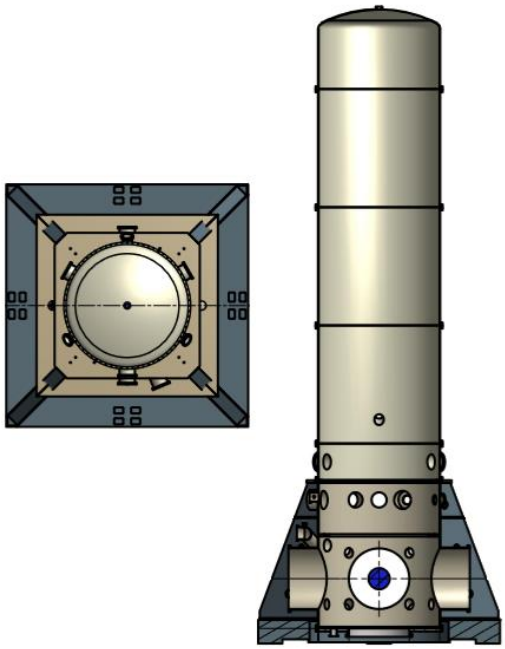

[fig1] Illustrated above is a diagram of both the top and side view of the West End tower. It can be seen in blue where the mirror would be positioned for AdV. Our attention is focused on this position when characterizing the magnetic fields and gradients inside the tower.

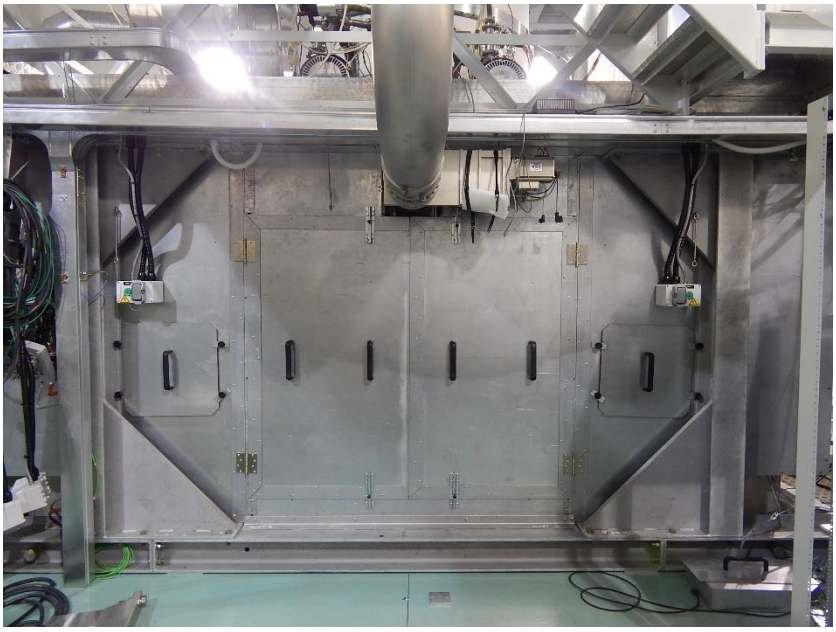

[fig2] Figure 2 is a photograph of the WE oven with its North wall in direct view. Access to the lower part of the tower requires only opening the oven doors.

2.3. Experimental Plan

Firstly, as previously mentioned, both the WE tower and oven are comprised of steel which is a weak ferromagnetic material; although, the oven material (Fe360) can carry some more significant residual magnetization. According to Faraday's Law of Induction, magnetic fields are generated by induced currents produced by vibrations of conductive materials. With that being said, we are aware that the WE tower and oven are subject to vibrations due to the seismic activity of the floor or impinging acoustic waves. The first experiment will investigate the magnitude of these vibration-induced magnetic fields of the WE tower and oven, as described in more detail in section 4.1.

Secondly, external magnetic fields induce Eddy currents within the bulk of WE tower by Faraday's Induction Law, which induce currents of their own and partially "cancel out" (at least locally) the external field. As a result, the magnetic field strength inside the tower should be reduced. This effect is referred to as the "shielding" of the tower. The magnitude of the magnetic shielding of the WE tower might depend on the position inside, but we are solely interested in the position of the mirror, which is a well-defined volume of 0.4x0.4x0.4 m^3 at the tower's center (65 cm above the inner floor of the tower). In addition to the WE tower, we also believe that the oven might contribute to the overall shielding of external magnetic fields; therefore, the second experiment will consist of measuring the transfer function between fields inside and outside the tower-oven conjunction and the oven alone (Sec. 4.2).

Lastly, as described by the equations of $\vec{F}$ and z_{mirror}, a force that displaces the mirror along z is associated with a magnetic field gradient $\nabla B'$, where the prime denotes "inside the tower". To measure this quantity, we will generate a well-known external magnetic field using a meter-wide coil. This injection will also allow us to understand and quantify how the tower spatially distorts this injection field at the volume specified where the mirror will be positioned. That is we will measure the magnetic gradient generated by the coil inside the tower along the z-axis. At first, the coil will be situated relatively close to the WE tower and then re-positioned far away (10 m) to also simulate the condition of far sources (Sec. 4.3). Ideally, we would need to repeat for different positions of sources around the tower.

3. Experimental Tools

3.1. Magnetometers

To extract the magnitude of the environmental or injected magnetic fields, we will use two magnetometers, each with their own advantages. The first is the MFS-06 (by Cooper Tools) which is 1 meter long, tube-like, and has very low intrinsic noise (better than 0.01 pT/√Hz at 10 Hz) which makes it suited to measure the field strength variations of the earth [ref2]. Although, it is quite heavy and requires re-positioning to readout all components (the 3 spatial dimensions) to a magnetic field. Therefore, due to its high sensitivity, we will use the MFS-06 magnetometer for the vibrational study of the WE tower and oven.

On the other hand, the second is a small, tri-axial magnetometer called the FL3-100 (by Stefan Mayer Instruments); it is about 10cm long by 2.5cm^2 and its intrinsic spectral noise is about 10pT/√Hz at 10 Hz [ref3]. The FL3-100 is portable and can read the 3 spatial components to a magnetic field within an accuracy of 0.5% [ref3]. Unfortunately, it is limited by intrinsic

noise at low frequencies. The tri-axial probe will be used for both shielding and distortion studies, with the injection signals being strong enough to overcome background noise. The probe will also be set up with a pole and aluminum bar where its configuration is later described Section 3.4.

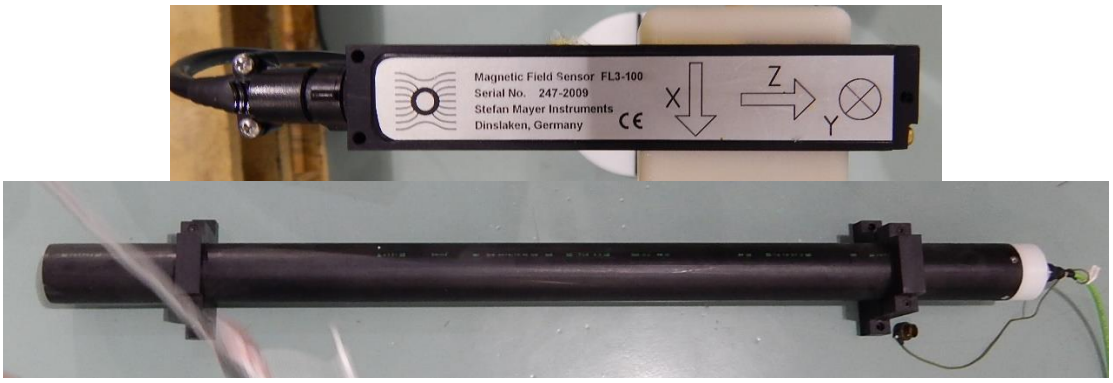

[fig3] The first image is the tri-axial magnetometer, FL3-100, where the arrows indicate the direction it will be receiving the signals from. The image below it is the MFS-06 magnetometer capable of measuring the earth's low frequency, field strength variations. Also note that the pictures are not to scale.

3.2. Data Acquisition and Analysis

The readout of the magnetometer signals is obtained using either the Virgo ADCs (Analog to Digital Converters) or a portable signal analyzer named the CoCo80 (by Crystal Instruments). Simultaneously, the CoCo80 is also used as the signal generator for the magnetic field injections.

Furthermore, analysis of the data requires multiple, custom built scripts using MATLAB R2013a. Functions such as "pwelch", "mschohere", "tfestimate", "polyfit", and some custom Virgo functions are incorporated into the scripts.

3.3. Injection Coil

For magnetic field injections, a custom built coil is used to inject sinus and pink noise signals to measure the WE tower's response to magnetic fields and gradients. The coil is inserted in a circuit via cable comprising of one constant-current power supply and amplifier, which can be piloted by one signal generator (we used the signal out function of the CoCo80). The limitations to this setup can be found in the Appendix, Sec. 5.1.

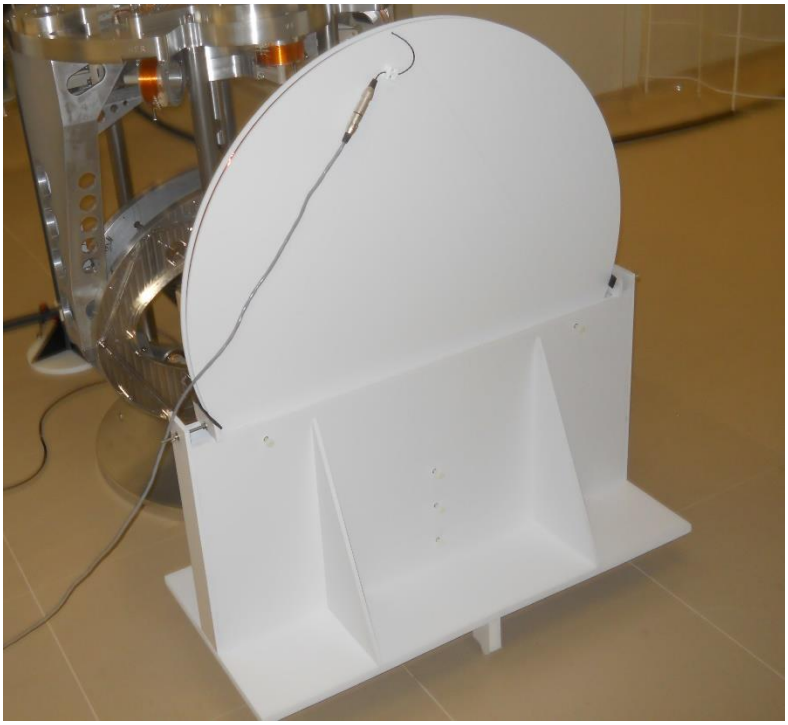

[fig4] Figure 4 displays the coil used for magnetic field injections. The coil is held by a rectangle mount and base where multiple screws can be used to adjust the height and vertical orientation of the coil. A current signal is added via the cable seen on the upper left region of the coil.

Table 3.3.1

Name	Value
Radius	r = 0.493 m
Number of turns	N = 50
Resistance	R = 3.6 Ohm
Inductance	L = 7 mH
Capacitance	C = 2.88 nF

[fig5] Table 3.3.1 displays all the known constants of the coil and all values for the equivalent RLC circuit (of the coil-cable-amplifier setup) found in the Appendix, Sec. 5.1.

3.4. Theoretical Field Strength along Axis of a Coil

In order to understand our experimental values, we will compare them to theory by using the magnitude of the magnetic field along the axis of a coil, which is as follows:

$$B_z = \frac{\mu_0}{4\pi} \frac{2\pi N r^2 I}{(z^2 + r^2)^{3/2}}$$

where μ_0 is the magnetic permeability, N is the number of wire turns, r is the radius of the coil, I is the current in the wire (measured), and z is the distance from the coil (measured). According to our study found in the Appendix, Sec. 5.2., we can match theoretical values up to an accuracy of 4.388%. The theoretical equation will be expressed as "Free-Field", which means in the absence of the tower, the magnetic fields behave as so.

4. Measurements

4.1. Vibration-Induced Magnetic Fields

According Faraday's Law of Induction, having the WE tower (which is made of steel) subject to vibrations should induce some magnetic fields to counter the change in flux. This is the topic of investigation and we would like to know how strong these induced magnetic fields are.

We used the MFS-06 for this study due to its high sensitivity, but we first checked if it can be affected by seismic activity itself. We laid the MFS-06 on the experimental hall floor, caring of placing it away from conductive materials which might produce vibration-induced magnetic fields. We also had a low frequency-sensitive accelerometer (Piezotronics, model PCB393B12) installed on the ground to measure vertical vibrations. We then shook the floor by jumping in proximity to both the MFS-06 and accelerometer. We find that, while we increased the floor's natural vibration by more than 10 times in the frequency range of interest (10Hz to 1kHz), the magnetic field measured by the MFS-06 (which was the typical magnetic field spectra of the experimental hall environment) did not change.

Focusing on the WE tower first, we laid the same magnetometer horizontally next to the tower (and inside oven with its doors open), along the beam direction. Then we attached the accelerometer to the tower's west flange. Firstly, we recorded the background seismic activity and magnetic noise due to the residual environmental noise of the hall. We then lightly knocked on the flange to induce vibrations for about a period of 10 seconds. Readings were recorded is synchronous way using the Virgo ADCs.

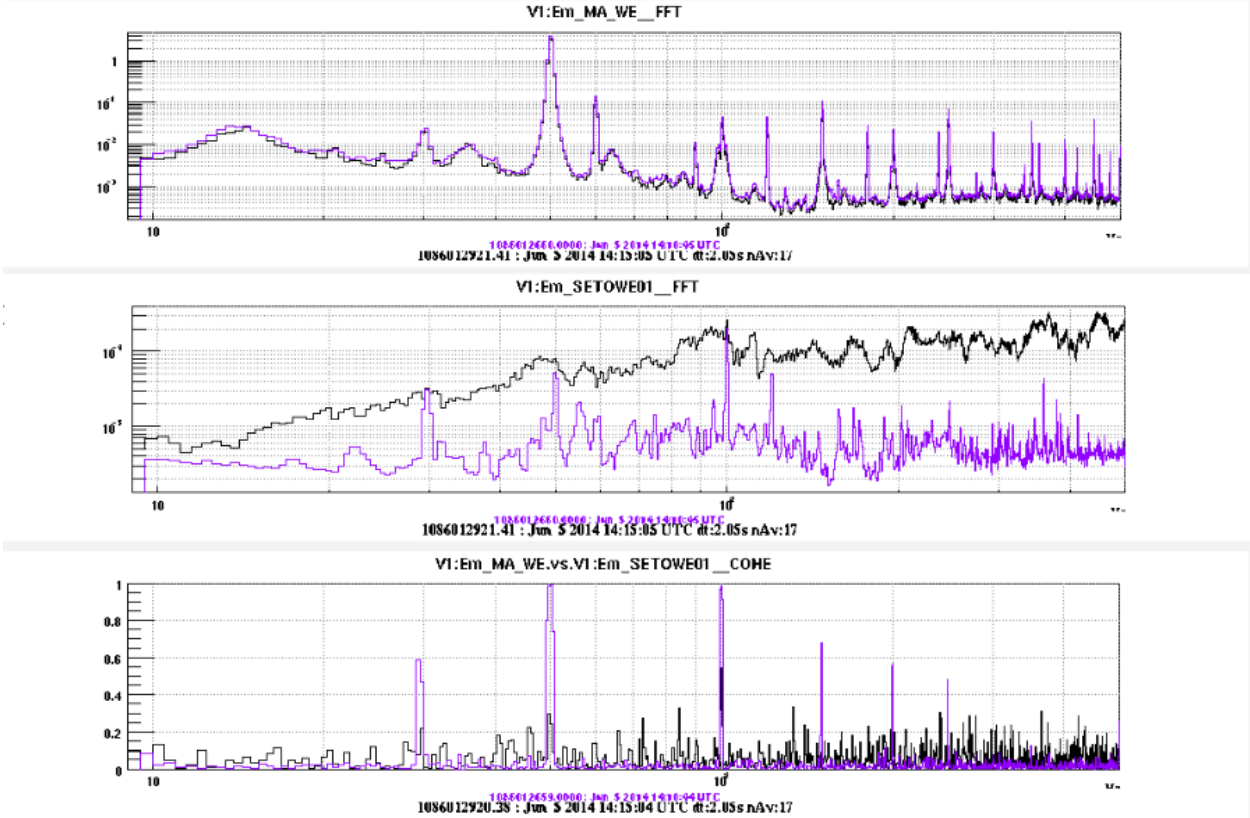

[fig6] Demonstrated from top to bottom is the magnetic field noise, seismic noise, and coherence plots from the vibration experiment as a function of frequency. The blue curve represents background noise, while the black curve denotes the readings from the knocking procedure. It can be seen that although there was increase in vibration, the magnetometer received little to no response.

Once all data was collected, we found that if there exists magnetic fields associated with the vibrations of the WE tower, then its effect is smaller than that of the dominant, environmental fields. In more detail, we increased the seismic activity of the tower by a factor of 10 (by knocking) in the whole frequency range of interest (10 Hz to 1 kHz); therefore, any magnetic fields associated by this movement should increase by 10 times (assuming linearity). Since no magnetic effect was observed, then we can conclude qualitatively that the vibration-induced magnetic fields are a factor of 10 below the environmental fields and considered “safe” for AdV.

On the other hand, the WE oven shares a different story. The same procedure was applied to the oven with the exception that the accelerometer was placed in rigid contact to the oven surface and the MFS-06 laid outside oven wall. We were careful to apply an increase in seismic noise by a factor of ten, so that its “background” noise would be roughly 10 times larger than that of the tower walls. Although, we found that the oven is much more sensitive to vibrations than the tower – mostly because it is far less rigid than the 13-ton chamber. When shaken, we measured a significant increase in magnetic noise, which we interpret as induced by oven vibrations.

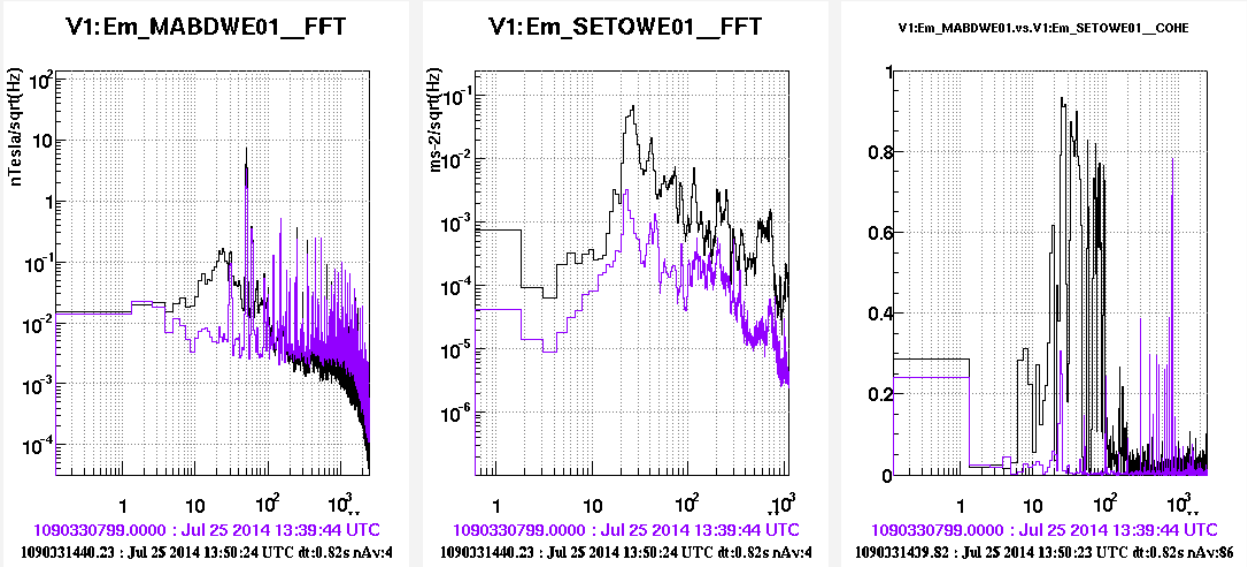

[fig7] The image now reads the magnetic field noise, seismic noise, and coherence from left to right (in the order listed). Once again, the blue curve represents background noise, while the black curve denotes the readings from the oven-knocking procedure. The MFS-06 magnetometer was quick to detect an effect of the vibration of the WE oven. Increasing the seismic noise of the oven by a factor of about 10 induced magnetic fields of the same factor.

We conclude that if both the tower and oven were subject to a common noise that would increase their vibrations by a factor of 10 or less, then the oven would induce magnetic fields 10 times stronger, while the tower would produce magnetic fields 10 times below the dominant noise. If all ovens behave as so, then its magnetic role is not “safe” for use in AdV.

4.2. Magnetic Shielding Study of the WE Tower and Oven

In addition to the quantifying the shielding effect of the WE tower, we wish to find out how much additional magnetic shielding the oven contributes to. Although we found out that the WE oven is sensitive to vibration-induced magnetic fields, this investigation will promote whether or not it is a good choice to remove each oven from their respective towers.

The experiment consisted of placing two tri-axial probes equidistant (2.545 m +/- 2cm) from the center of the injection coil, but at opposite ends. One probe resided inside the WE tower at the position of the supposed mirror while the other resided outside; both probes had their z-components facing perpendicular to the plane of the coil. Note that both probes described were calibrated in respects to each other; the calibration experiment can be found in the Appendix, Sec. 5.3.

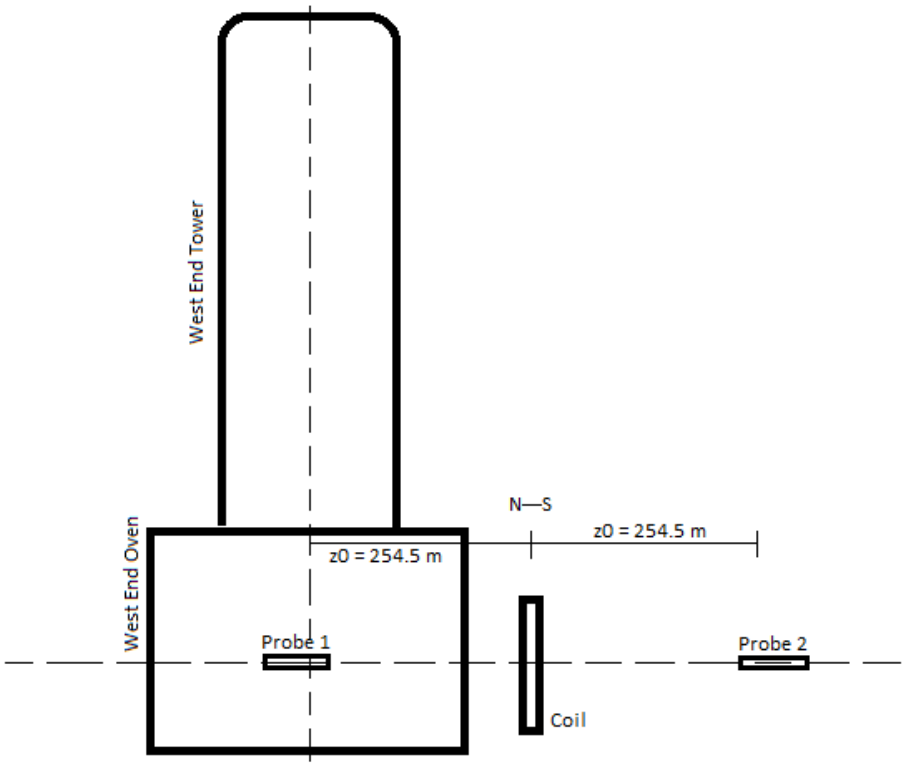

[fig8] Pictured above is rough diagram (not to scale) of our experimental setup described previously. The distance "z0" stretches from the center of the z-arrow on the probes to the middle of the coil.

After the setup, we injected a pink noise current signal of 0.1 Amps while the oven doors were closed and then started measuring data using the Virgo ADCs. In order to disentangle the possible shielding contribution of solely the oven, we repeated the procedure with the oven doors open so that the coil faced the tower alone.

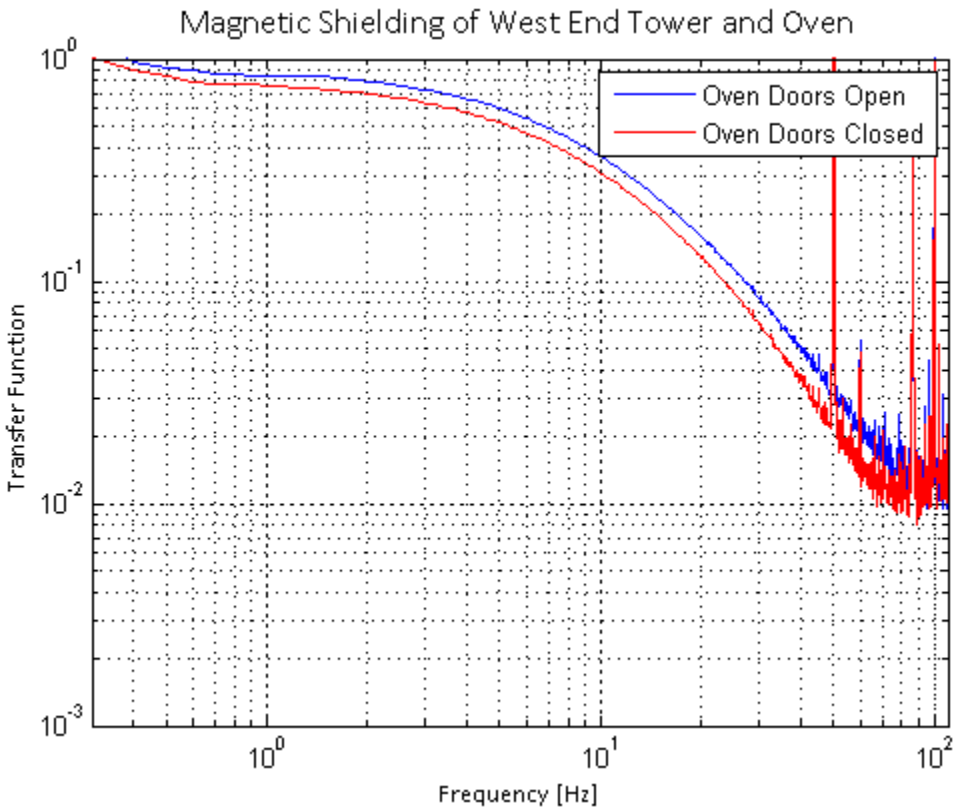

[fig9] Illustrated above is the transfer functions between magnetic fields inside and outside the WE tower and oven, as a function of frequency. The blue curve represents the magnetic shielding due to the tower-oven conjunction, while the red curve represents the shielding due to only the tower. The frequency range shown is the region where coherence between the current and the magnetic fields was above 0.8.

Furthermore, it can be seen that overall the shielding of magnetic fields increases with frequency, but having the oven doors closed allows for just a bit more shielding. At 10 Hz, the shielding increases by about 19% when the oven doors are closed. The oven's shielding is more or less independent on frequency when compared to the tower. On the other hand, this gain in shielding capacity is indeed small, thus not high enough to compensate for its high sensitivity to vibration-induced magnetic fields.

4.3. West End Tower Distortion of External Magnetic Fields

As described earlier, Eddy currents induced in the bulk of the towers spatially distort the external magnetic field lines as they transmit through. We wish to understand this effect by investigating the gradient inside the chamber and compare it with theory.

Moreover, we are interested in the z-component of the gradient generated at the mirror position inside the WE tower by both close sources (aka, "Near-Field") and distant sources (aka, "Far-Field"). Having that said, we conducted two experiments: Near-Field simulation by placing coil 2.5 meters away from mirror, and a Far-Field simulation by placing the coil 10 meters away from mirror position. Note that displacing the coil further away causes the generated signal to be too weak and difficult to measure.

To initialize the experiment, we placed the injection coil at a distance of z_0 = 252.5 cm away from the center of where the mirror would lie, which is the position where the tri-axial magnetometer will be initially. The coil was positioned outside (and relatively close to) the chamber walls where its axis aligned to the laser beam (not on) and probe; we estimate our positioning accuracy to about 2 cm.

For the Far-Field measurement, we instead set z_0= 10 m. In this case, the alignment was more critical and using a simple measuring tape would carry too large an uncertainty, thus we asked support of the EGO topography experts, who (by means of one professional laser level tool) aligned the coil with an accuracy estimated to be less than 1 cm.

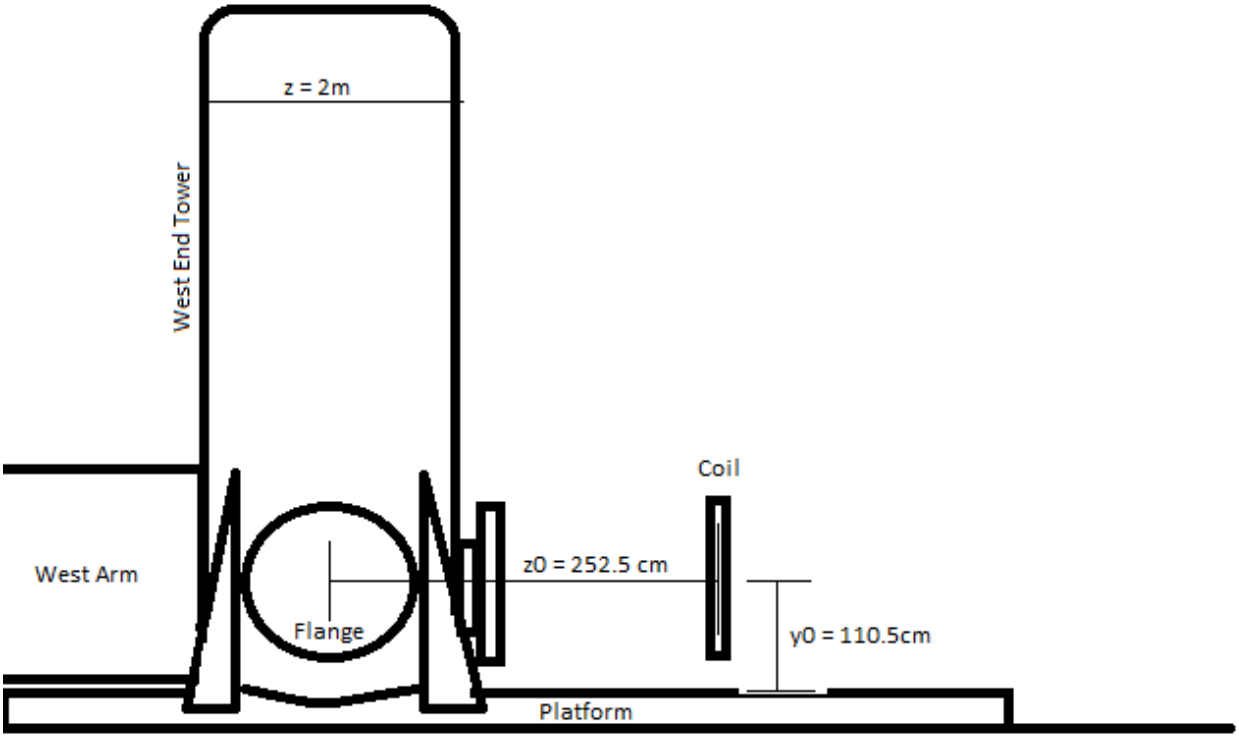

[fig10] Figure 10 is a rough diagram of our experiment, which is not to scale and viewed at the N-S direction. The coil resides outside the tower in front of the west flange while the magnetometer will be pointing towards it inside the chamber. Accurately placing the coil meant centering it towards the west flange since it is centered to the center of a test mass; therefore, we assume that the position of the west flange has very little error.

Once everything was positioned carefully, we injected into the coil circuit a sine current signal of 0.574 A amplitude at a 10-Hz, 25-Hz, and 40-Hz frequency for the Near-Field simulation, and a 3 A amplitude at a 10-Hz frequency for the Far-Field simulation. We did not inject any higher frequencies for the Far-Field simulation because we are limited by the shielding and distance from the tower. Although we could increase the current to compensate, we aware that the high current can generate enough heat to alter constants in the circuitry (like the resistance) of the coil and cable. On the other hand, the scanning procedure involved moving the probe inside the chamber along z (beam direction) by 2.5-cm (Near Field) and 5-cm (Far Field) steps. At each

probe position, we recorded the readings of the amplitude of the magnetic field (as measured by the z-component of the probe) with the CoCo80. We also read out the amplitude of the current signal to check that it kept constant during the scanning procedure; we observed a maximum deviation of 0.1%. After gathering the data, we placed them into specific MATLAB scripts that will allow to carry out the analysis of the WE tower distortion.

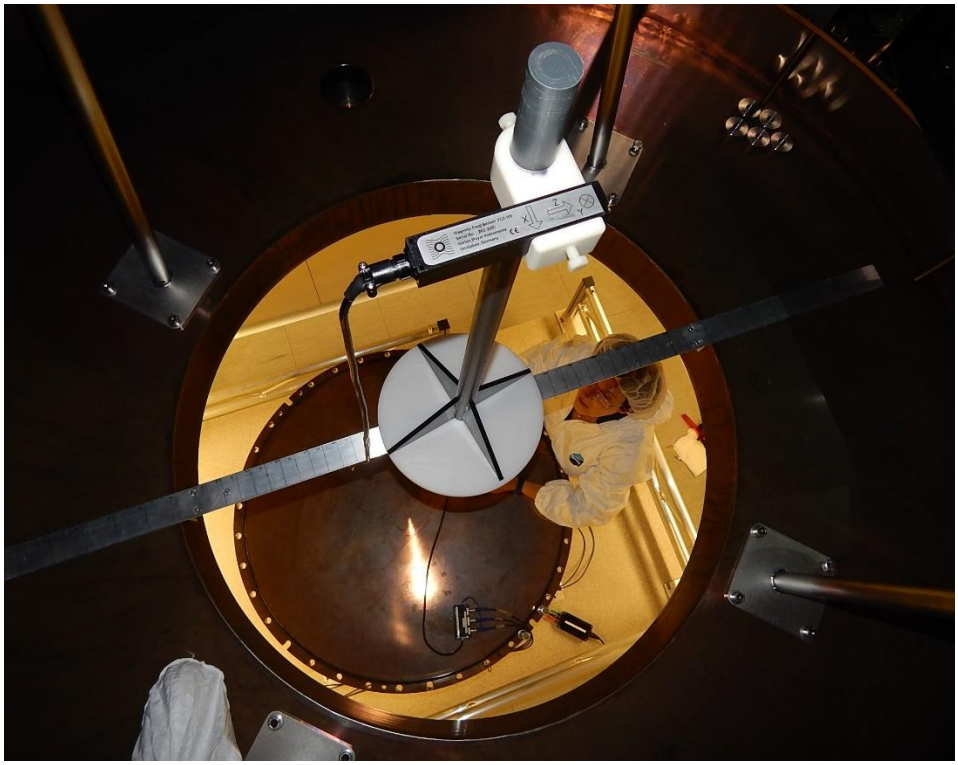

[fig11] This photograph was taken inside the WE tower, where the setup for the z-scan is shown. A custom-made aluminum bar was used as support for the probe/pole, and used to precisely move along the beam direction. We tested previously if the conductive nature of the aluminum bar would alter readings, but as described in the Appendix, Sec. 5.2, it did not influence the readings. The present position of the FL3-100 seen will be the position of the AdV mirror – the position where we want to quantify the magnetic field gradient. Note that the scanning of the z-axis or axis of coil is only within the tower.

Here below we show the measured magnetic fields and gradients for the Near-Field and Far-Field experiments, where we compare each curve to Free-Field, theoretical values using the equation for the magnetic field along the axis of a current loop. Note that the gradients are computed differentiating field values (i.e. using the MATLAB “gradient()” function).

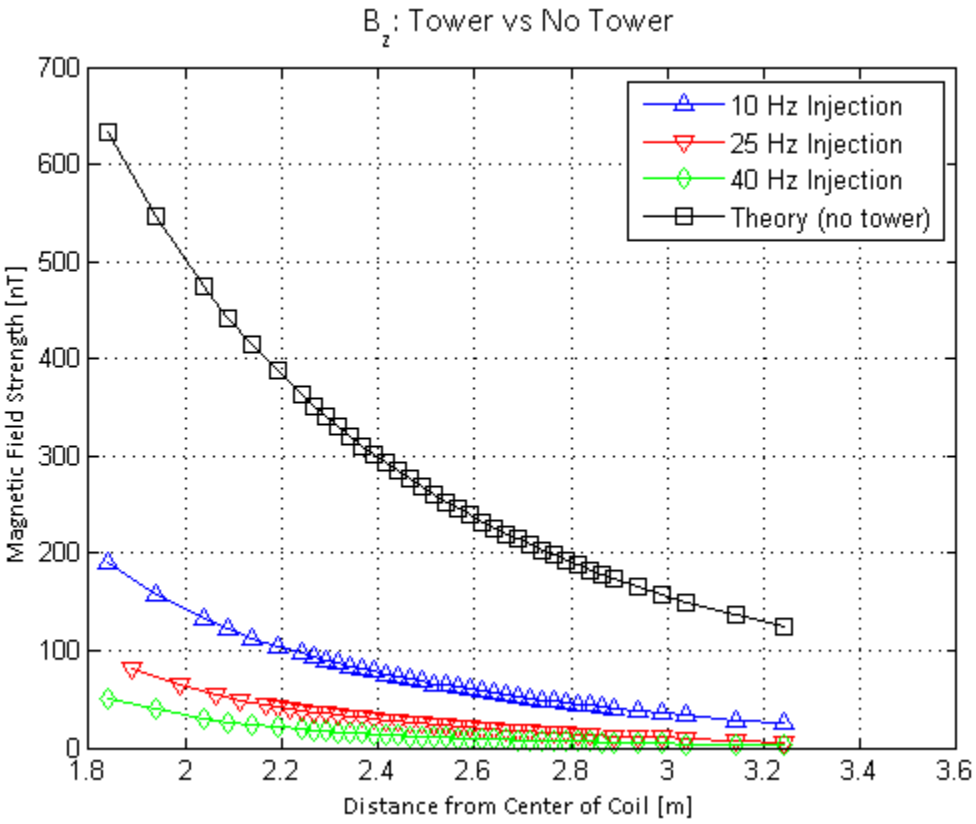

[fig12] Figure 12 illustrates the z-component of the Free-Field magnetic field as a function of distance (black). It also displays all the z-scans for 10-Hz, 25-Hz, and 40-Hz sine injections which are compared to theory. Despite the tower, the experimental values behave the same way as the theoretical values; they all decrease in magnitude as we get further away from the coil. Note that the nominal position of the mirror (z_{mirror}) is at 2.525 m.

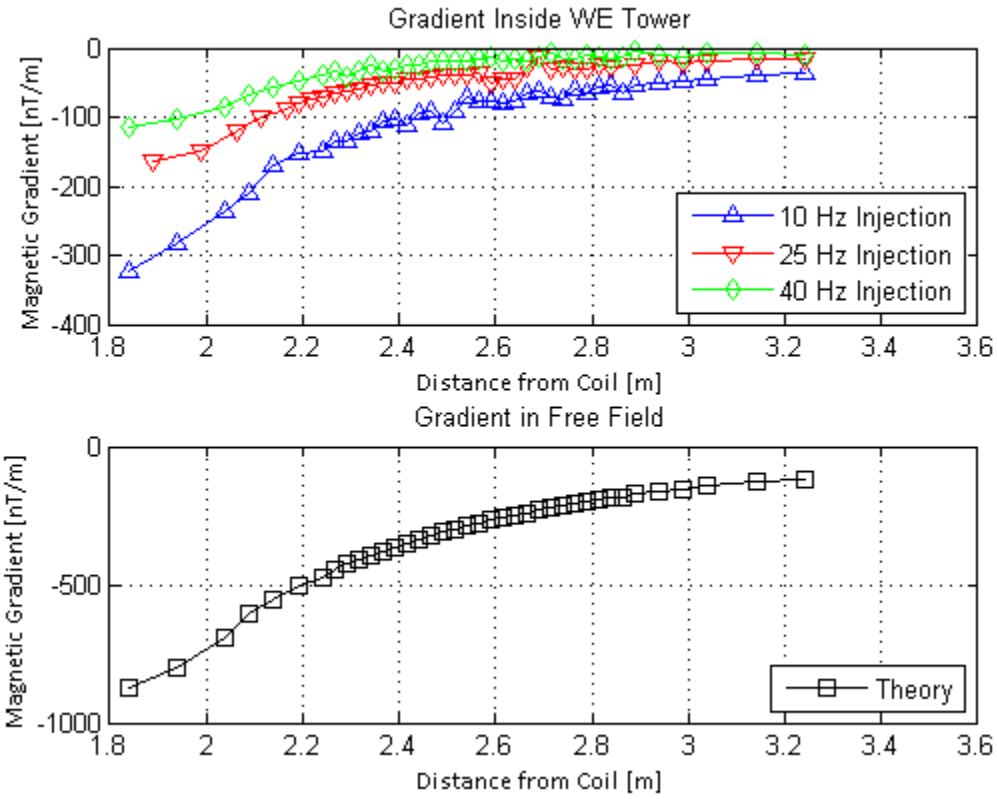

[fig13] In both plots, the gradient of the magnetic field is a function of distance. All experimental gradients inside the tower decrease as we get further away from the injection coil as expressed by theory. This makes sense because field lines get less and less steep as we get further away from a current loop. Again, the nominal position of the mirror is 2.525 m.

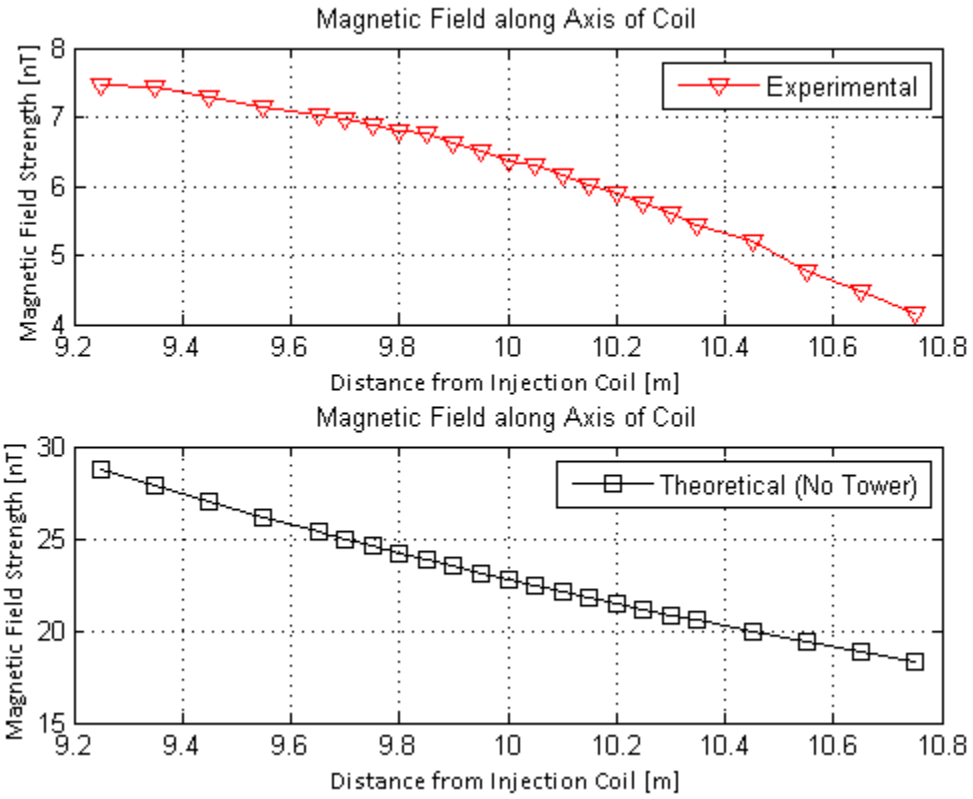

[fig14] Figure 14 demonstrates the magnetic field strength as a function of distance for a near-uniform field injection, with z_{mirror} being 10 meters (red, top), comparing it to the free field (black, bottom). Again, we notice the shielding nature of the WE tower in effect, but we also notice that the experimental field strength decreasing more slowly than theory.

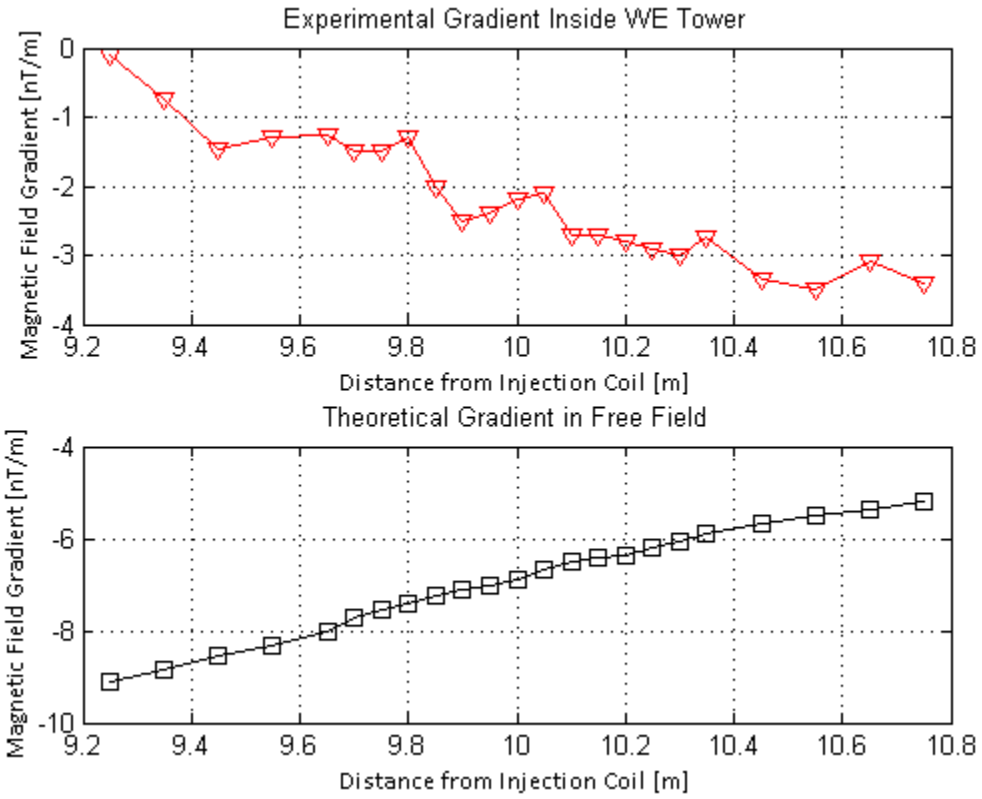

[fig15] From figure 15 we see that the experimental, magnetic field gradient increases with distance rather than decreasing like theory proposes. (Nominal position of mirror is 10 m.)

The gradient itself does not change with the intensity of the injected field. Instead, we seek for a quantity that can characterize "how much" the WE tower distorted the injected field while being independent from the intensity of the injected field. Since the gradient scales proportionality with the intensity of the injected field (i.e. given: $B_2 = c*B_1$, then: grad B_2 = c*grad B_1), it seems that a good quantity is the ratio between the measured gradient inside the tower and the Free-Field magnetic field values:

$$MFDF = \frac{\nabla B_z'}{B_z}$$

where $\nabla B_z'$ denotes the z-component of the magnetic gradient inside the tower and B_z denotes the z-component of the magnetic field in absence of the tower. The Magnetic Field Distortion Factor (MFDF) was introduced and derived in an earlier paper concerning the same issue [ref4].

Furthermore, figures below show this quantity (triangles) computed for the injections in the Near-Field (Figure 16) and the Far-Field (Figure 17). Each MFDF curve includes a fit line, whose computation is described later on.

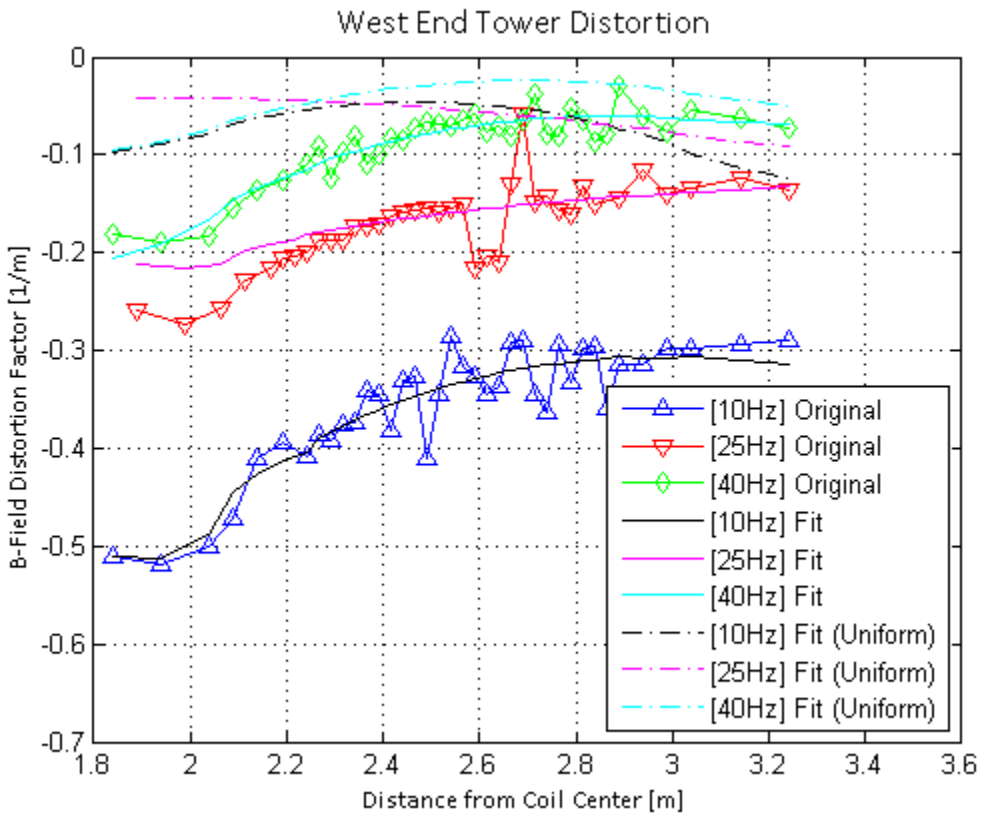

[fig16] Shown above is the Magnetic Field Distortion Factor (MFDF) as a function of distance for the WE tower, Near-Field injections. In the legend, “Original” represents the first interpretation of the MFDF from an earlier paper, while “Fit” denotes the second interpretation (best fit curve), and then finally “Fit (Uniform)” denotes the second interpretation in the case of a uniform magnetic field.

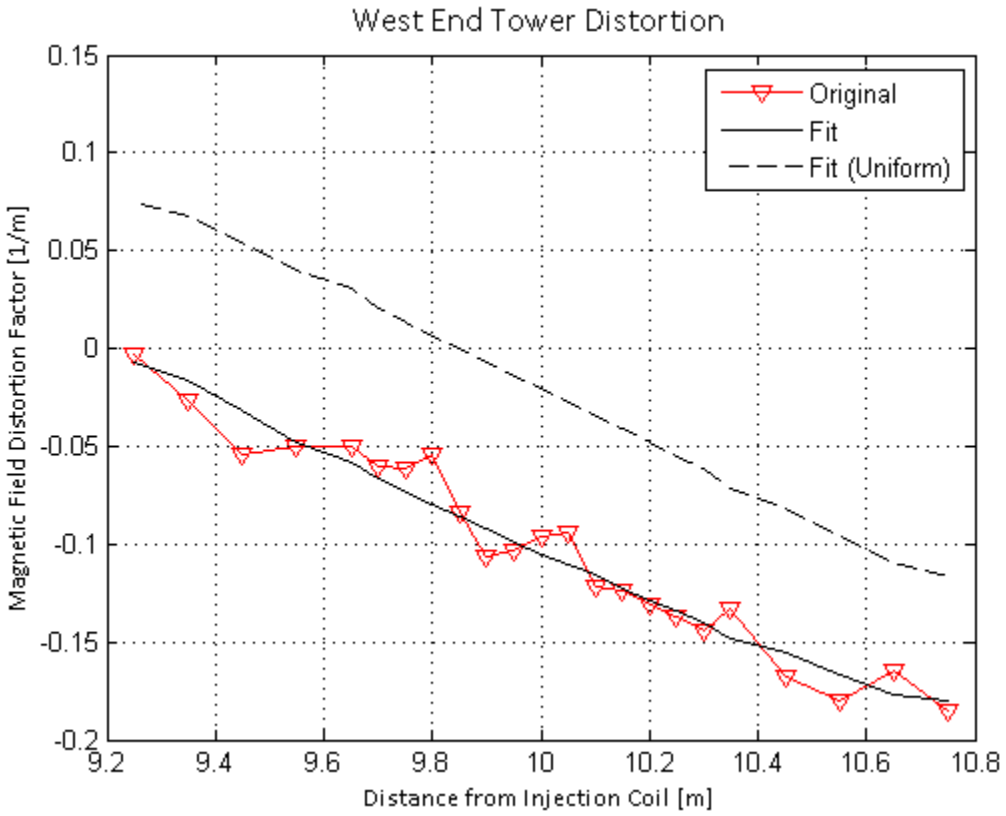

[fig17] WE tower distortion for the case of a Far-Field injection (10Hz). Both "Original" and "Fit" curves display the same behavior, while "Fit (Uniform)" also does so, but its difference in magnitude is due to being a perfect uniform field. On the other hand, "Fit (Uniform)" goes from a positive distortion to a negative distortion which may imply that the direction of distortion changes with distance.

The fit lines applied to the curves were formulated using the derivation of the MFDF. This formulation relies on the assumption that the distorted field inside the tower along z (denoted with "prime") is proportional to the injected field along z (as we will discuss later, we think this hypothesis does not strictly hold for the Near-Field case). Its derivation is as follows (again let the prime denote "Inside the Tower"):

$$B_z' = K(z) \cdot B_z$$

$$\frac{\partial B_z'}{\partial z} = \frac{\partial K}{\partial z} \cdot B_z + K \cdot \frac{\partial B_z}{\partial z}$$

$$Let\ \frac{\partial}{\partial z} = \nabla\ ,\therefore\ \nabla B_z' = \nabla K \cdot B_z + K \cdot \nabla B_z$$

$$\frac{\nabla B_z'}{B_z} = \nabla K + K \cdot \frac{\nabla B_z}{B_z} = MFDF$$

where $K(z)$ is a polynomial of the nth-power. The variable K is essentially the ratio between magnetic fields inside and outside the tower, as a function of distance. In addition, the last equation expresses two terms, the first (∇K) is the distortion due to the tower itself, while the second term ($K \cdot \frac{\nabla B_z}{B_z}$) is the contribution of distortion associated with the source itself. We see that for an ideal source of uniform field lines (i.e. ∇B_z= 0) the second term goes to zero and the MFDF coincides with the distortion factor of the tower itself.

Furthermore, the term $K(z)$ can be extracted from our experimental data and then fitted to an n-order polynomial to express the new variable, K_{fit}. $K(z)$ and K_{fit} are shown for each z-scan in the figures 18 and 19.

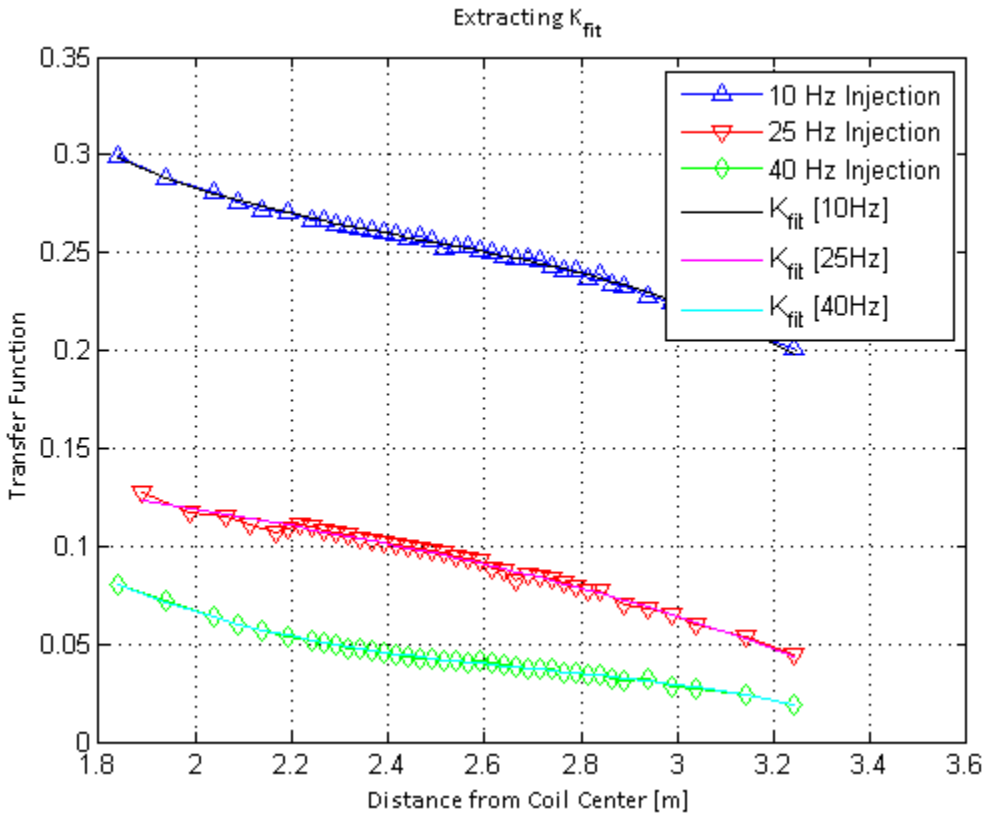

[fig18] Figure 18 displays the function K for the Near-Field injection. The data is fitted with 3rd power polynomials. Also note that for higher frequencies the transfer function is smaller, which supports the magnetic shielding study of the tower-oven conjunction.

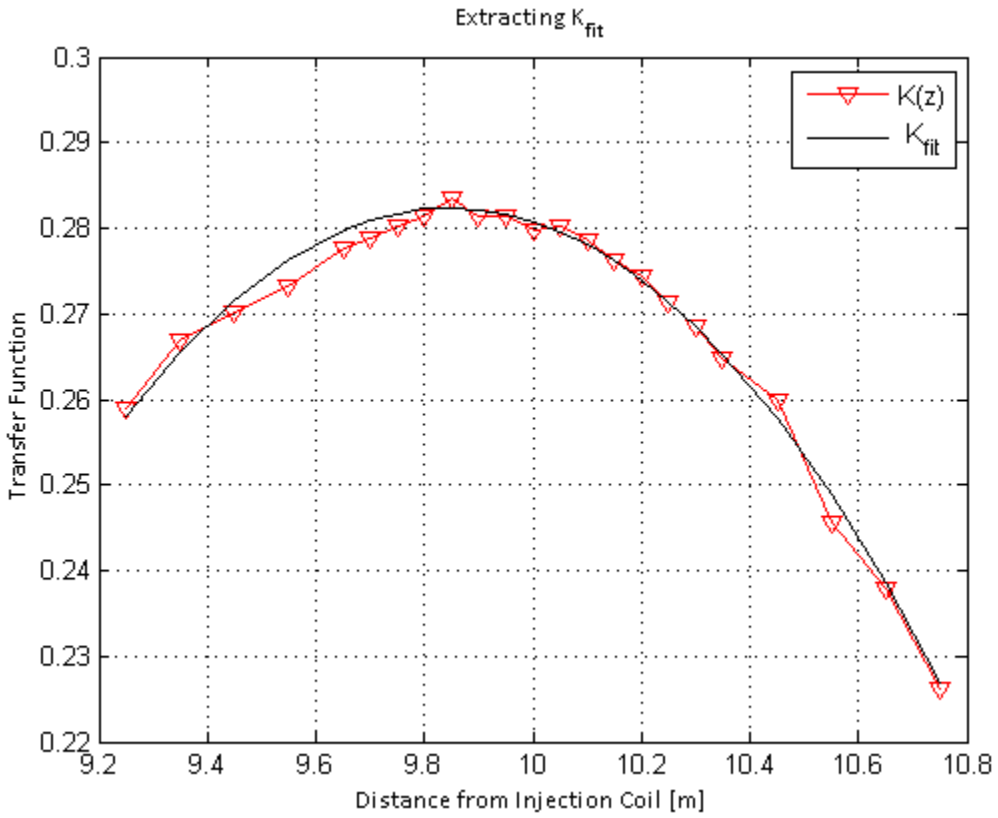

[fig19] The K function for the Far-Field injection also as a function of distance. Although it can be seen by eye, the extraction of K_{fit} from experimental data revealed that $K(z)$ is a polynomial of the 2nd power. Figure 18 is also suggesting that the transfer function inside the WE tower can be the same for two different positions, when there exists an external uniform field.

In summary, we are interested in the values of field distortion at the location of the mirror magnets (see Sec. Technical introduction). Also note that, we are interested in absolute values since magnetically induced strain noise does not depend on the direction the mirror is displaced or in other words, strain is produced whether the magnetic force is pulling or pushing the mirror. Thus, we choose the following, conservative, way to summarize results: we take the maximum absolute value over a z-range which goes from -0.2m to +0.2m from tower (mirror) center (in Table 4.3.1) and then also in the wider z-range from -0.4 and +0.4m from tower (mirror) center (in Table 4.3.2).

Table 4.3.1

Injection	Bz [nT] Free-Field	Bz' [nT] inside tower	grad(Bz') [nT/m]	MFDF [1/m]	grad(K) [1/m]
Near-Field, 10Hz	320	84	120	0.38	0.06
Near-Field, 25Hz	320	32	56	0.18	0.05
Near-Field, 40Hz	320	15	35	0.11	0.04
Far-Field, 10Hz	21	6	2.5	0.12	0.05

[fig20] Table 4.3.1 displays all variables of interest from a z-range of -0.2m to +0.2m from mirror center for each injection study. These values will be used to compare with a computational simulation of the "cage" (described later) done by another research team in Rome, Italy.

Table 4.3.2

Injection	Bz [nT] Free-Field	Bz' [nT] inside tower	Grad(Bz') [nT/m]	MFDF [1/m]	grad(K) [1/m]
Near-Field, 10Hz	414	112	180	0.45	0.08
Near-Field, 25Hz	414	50	100	0.40	0.06
Near-Field, 40Hz	414	24	60	0.14	0.03
Far-Field, 10Hz	25	7	3	0.14	0.07

[fig21] Table 4.3.2 again displays all variables of interest from a z-range of -0.4m to +0.4m for each injection study. These values will be used to compare with a computational simulation of the "cage" (described later) done by another research team in Rome, Italy.

Experimental values in Tables 4.3.1 and 4.3.2 provide a tentative evaluation of the magnetic field distortion by the mirror vacuum chamber ("tower"). We remind the reader that: (1) column "MFDF" of Tables 4.3.1 and 4.3.2 are a measure of the gradient field per unitary field strength produced inside the tower by one (specific) near source which is the 1m aperture coil placed at 2.5m from the tower center (that is indeed a quite sizable source); (2) instead, column "grad(K)" provides a measurement of the same quantity for one Far-Field source (i.e. uniform field at the tower location"). These are both interesting results because case (1) allows to "size" the effect on dark fringe noise of near or large size sources (such as vacuum pumps) and case (2) allows to "size" the effect of distant or small-size sources (which is indeed the majority of sources in AdV experimental halls).

One clear limitation of our measurement is that we probed just two positions and orientation of the magnetic field source in the hall with respect to the tower. We chose the orientation where the magnetic field is the strongest along the beam line direction (which corresponds to the strongest distortion along z), but it would be useful to repeat the experiment with different orientations and locations of the coil, both in Far-Field and in Near-Field type of injections.

Here are concluding remarks about results shown in Tables 4.3.1 and 4.3.2: (1) We find an indication of a frequency dependence of the field distortion (as we noted for the residual field strength inside the tower), which tends to reduce with increasing frequency. We believe that this might be explained by the fact the intensity of induced Eddy currents increase with frequency. This effect indeed is more evident for the Near-Field sources (column "MFDF" in Tables 4.3.1 and 4.3.2) than for the Far-Field ("grad(K)" in Tables 4.3.1 and 4.3.2). (2) The Far-Field measurement of grad(K) (which was only 10 Hz) does agree with that extracted from the Near-Field at 10 Hz (0.05 m^-1 and 0.06 m^-1 respectively in Table 4.3.1, 0.07 m^-1 and 0.08 m^-1 resp. in Table 4.3.2). This seems an indication of the trustworthiness of our analysis method (see derivation of MFDF). (3) The Far-Field values found in 4.3.2 can be compared with

the EM Comsol simulation work done for the mirror "cage" [ref1]. In this work it is estimated the maximum distortion produced by Eddy currents in the cage structure induced by external uniform fields (they simulated uniform fields impinging the cage from different directions and took the max value of distortion which indeed was produced by uniform fields aligned along z) . Figure below is taken from EM Comsol simulation:

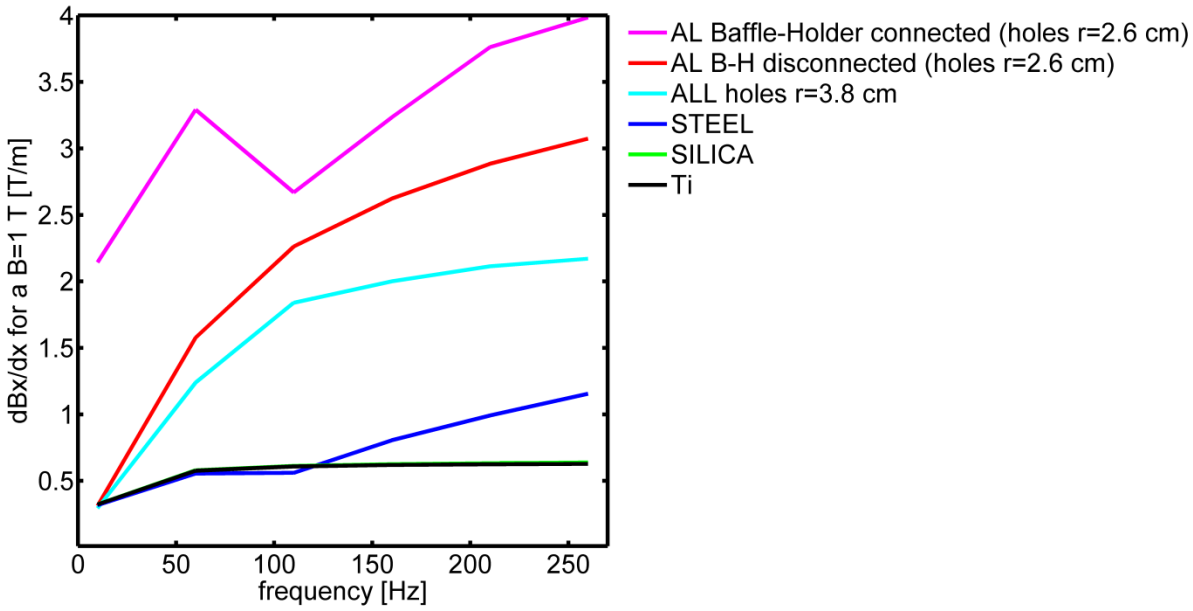

[fig22] Red line of above graph refers to the case of "disconnected Aluminum baffles" which represents the configuration of the actual AdV beam-splitter (BS) mirror "cage". We see they find distortion values that go from $0.3m^{-1}$ at 10 Hz to $1.5m^{-1}$ at 40 Hz. We assume field-distortion effects from the cage and the tower (our measurement) add linearly. Our most conservative measured number for the "tower" (Far-Field) is or order of $0.08m^{-1}$ (Table 4.3.2). This looks almost negligible with respect to the cage contribution. In the same paper ([ref1]), a preliminary evaluation is made of the strain noise associated to the measured cage magnetic field distortion, and it is found to be about a factor 5 to 10 below the AdV sensitivity. Based on this, we might tentatively conclude that the tower induced magnetic field gradients at the mirror induced (by Far-Field sources with the same typical strengths we had in Virgo) gives a negligible contribution to AdV sensitivity.

(4) Near-Field sources can produce (at the mirror location) gradients that are quite larger than Far-Field sources (column "gradBz'" in Tables 4.3.1 and 4.3.2) and as well larger field distortions or gradients per unitary field (column "MFDF"). The numbers in Table 4.3.2 can be used to do a tentative prediction of the noise produced in AdV dark fringe for one "test" extended source (similar to the coil) and positioned in the proximity of the tower (see figure 23).

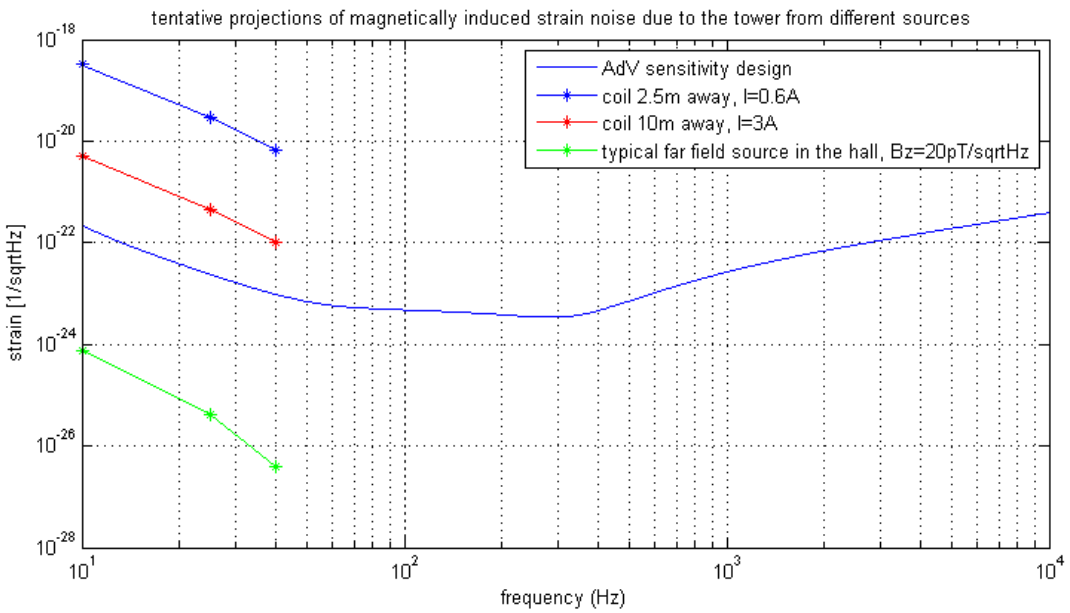

[fig23] Figure 23 illustrates where our measurement's predicted strain noise fall in respects to the AdV sensitivity.

From figure 23, it can be seen that all experiments conducted (using artificial injections) indicate that strain noise induced by magnetic fields and gradients are a factor of 100 to 10000 times above AdV design , which is considered "safe".

5. Appendix

5.1. Limitations with Coil-Cable-Amplifier Setup Used for Injections

Before conducting measurements, we studied the coil-cable-amplifier setup in order to find out if we are limited by anything due to its composition or circuitry. Its equivalent circuit is as follows:

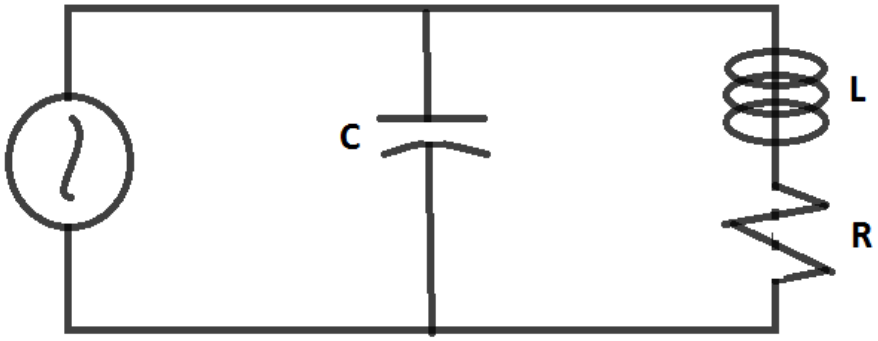

[fig24] The equivalent circuit of the coil-cable-amplifier setup. It is an RLC circuit where the capacitor is in parallel with the inductor and resistor. The values of these constants can be found in Table 3.3.1.

Additionally, we studied the impedance of the coil-cable-amplifier setup for a wide range of frequencies.

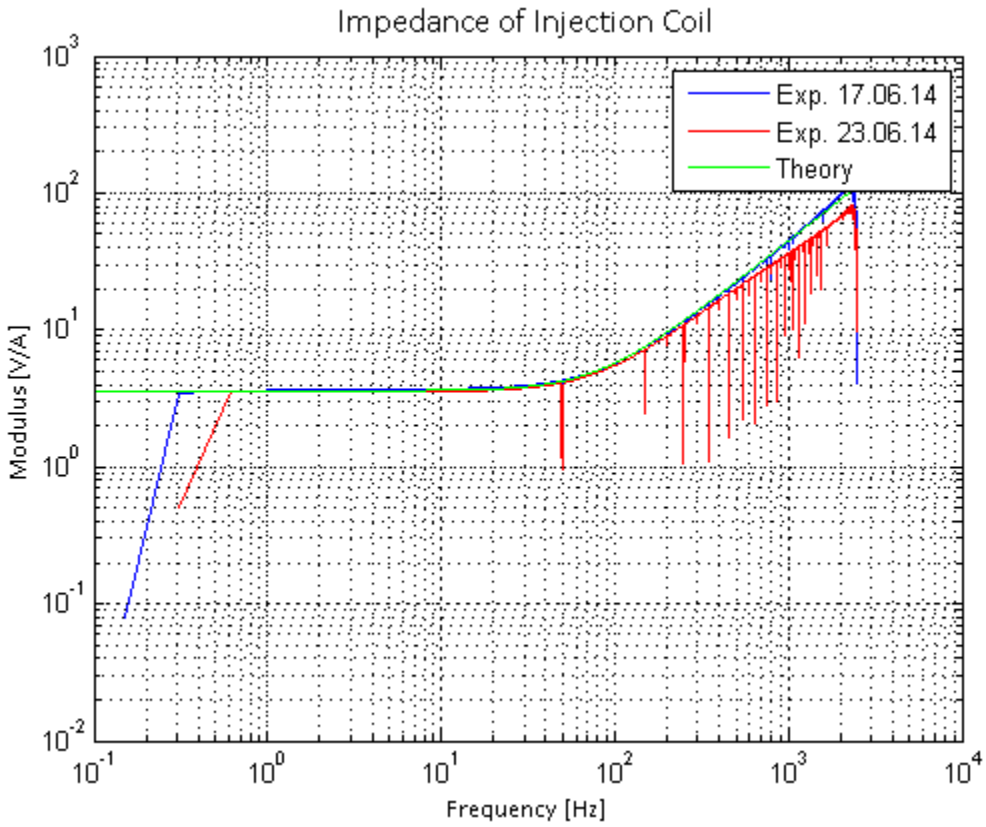

[fig25] The plot above shows the modulus of the impedance as a function of frequency with respect to theory. After two trials, we notice a discrepancy at higher frequencies of about 350 Hz and above. We believe there has been an increase in capacitance because the impedance due to the capacitor in inversely proportional to its capacitance. Although we were consistent with our experiment, we are still unsure of this mysterious behavior. Our only limitation is at high frequencies where the current drops significantly after 100 Hz; however, we are only concerned with frequencies between 10 Hz and 100 Hz because we expect this region of magnetic noise to affect the AdV sensitivity the largest.

5.2 Accuracy in matching Theoretical Values

It is critical for the distortion study to understand how the magnetic field lines are supposed to behave in the absence of the tower. The theoretical equation for the magnitude of magnetic fields along the axis of a coil grants us this interpretation. Before using the equation in the distortion study, we must first find out how close we can experimentally reproduce theoretical values.

For starters, we injected a 25-Hz sinus signal and then placed the magnetometer (held by a pole) in front of the coil from a distance of a little above 3 meters. We then scanned the axis of the coil by displacing the probe and pole at 10 cm steps. It is important to note that the

scan was conducted without the presence of other potential sources of EM noise and the magnetometer was positioned to center the axis of the coil. Moreover, the scan was repeated with the use of an aluminum bar (attached to the base of the pole) in order to check if the conductive nature of the aluminum would alter results. The purpose of the aluminum bar was to serve three goals: displace the pole smoothly and accurately by avoiding abruption, fit perfectly within the inner gap of the tower (where the mirror would hang), and to be strong enough to avoid bending due to the weight of the pole. After finding out that there exists very little discrepancy between results from the previously mentioned scans, the scanning procedure was once more repeated with the aluminum bar, this time to compare to theory. The error due to experimentation was 4.388%.

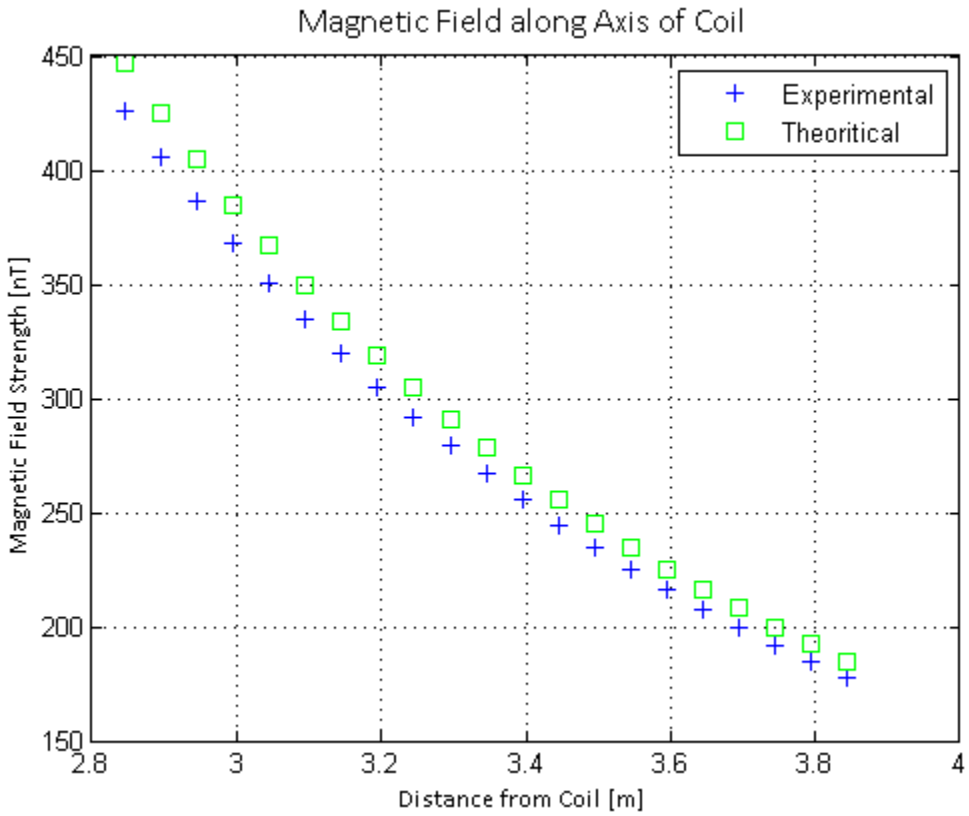

[fig26] Figure 26 displays the magnetic field strength as a function of distance with each point representing a 5-cm step. The discrepancy between the experimental and theoretical values was only 4.388%. Assuming that the FL3-100 and CoCo80 can read accurately, we believe are source of error spawns from the attempt to align the magnetometer to the center of the injection coil.

5.3. Calibrating the two FL3-100 magnetometers

In order to accurately compare the readings of both tri-axial probes used in the tower-oven shielding study, we wanted to make sure they could both read the same values from a source. This involved placing both probes on top of each other with their z-components facing the injection coil from a distance of about 5 meters. Although this experiment was conducted

for each component (x, y, and z), we were only concerned with the calibration (if any) of the z-readings. Furthermore, centering the probes to the axis of the coil was not critical because we were only interested if they could read the same value. Both probes were taped on top of each other for further accuracy in the position of z, and then a pink noise signal was injected into the coil using the CoCo-80.

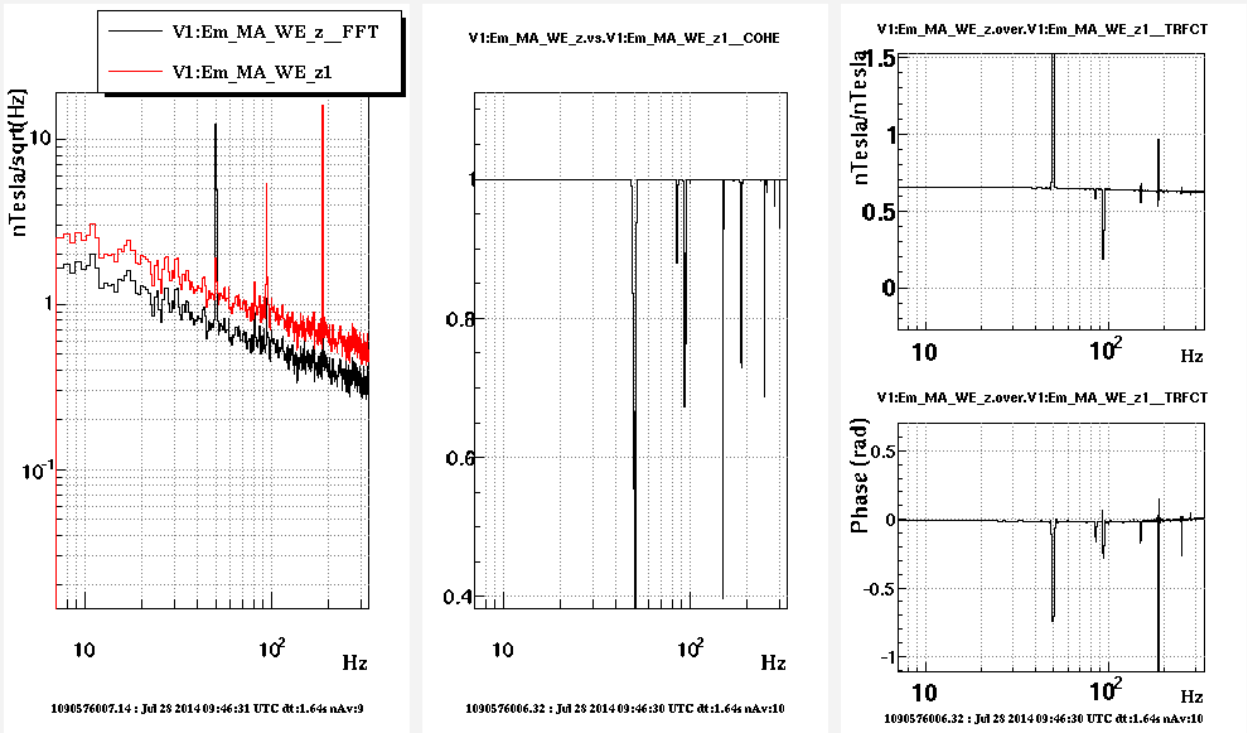

[fig27] From left to right are magnetic noise, coherence, and transfer function plots as a function of frequency. The range specified is where the coherence was nearly 1. Probe "z" laid on top of "z1"; although, which one was on top did not matter, because we repeated the experiment with "z" and "z1" swapped, and reproduced the same results. In addition, it was found that values from "z" were a factor of 0.65 times the values from "z1" at the same frequencies.

The transfer function between the readings of both probes indicated that there was a discrepancy in their readings. Although slightly unfortunate, the solution is implementing a calibration factor in the MATLAB script used for the shielding study. The readings from the probe inside the WE tower needed a calibration factor of about 1.54 in order to be accurately compared to readings from the probe outside the WE tower.

6. References

[ref1] Chincarini, A., *et al*. (2014). "AdV-PAY: XXXXXX," INFN, Sezione di Genova, I-16146 Genova, Italy. (Work in progress)

[ref2] Matzander, U. “MFS-06: Product Manual,” Cooper Tools, D-38120 Braunschweig, Germany

[ref3] “Triaxial Magnetic Field Sensor FL3-100,” Stefen Mayer Instruments, D-46535 Dinslaken, Germany

[ref4] Fiori, I., *et al*. (2014). “Tentative estimate of critical value of the magnetic field distortion factor at AdV mirror actuation magnets,” VIR-0171A-14, EGO, Cascina, Italy.